JOURNAL OF CATALYSIS 36, 81–92 (1975)

Structure and Catalytic Activity of MoO_3·Al_2O_3 Systems

I. Solid-State Properties of Oxidized Catalysts

N. GIORDANO,* J. C. J. BART, A. VAGHI, A. CASTELLAN, AND G. MARTINOTTI

Montedison, Research Center of Bollate (Milano), Italy

Received October 2, 1973

Supported MoO_3 on Al_2O_3 catalysts containing up to 30 wt% MoO_3 have been studied by various chemical–physical techniques in a wide temperature range (110–700°C). Bulk and surface structure differ considerably depending upon calcination temperatures. For samples activated at 500°C evidence is presented for a monolayer deposition up to about 15–20 wt% MoO_3: the chemisorbed molybdenum species, present in the uncalcined dried catalyst, interact with the carrier to form stable alumina–molybdic acid complexes at the surface, having a tetrahedral oxomolybdenum configuration in the MoO_3 poorest catalyst and a polyanionic mixed tetrahedral–octahedral structure in the medium composition range. With increased MoO_3 concentration part of the molybdenum is incorporated in octahedral interstices of bulk γ-Al_2O_3 while $Al_2(MoO_4)_3$ is formed and unreacted MoO_3 is left behind as clusters. The octahedral [MoO_6] species are considered to be a possible precursor of the $Al_2(MoO_4)_3$ phase. The effect of increasing temperatures is that the species mentioned above are present at lower concentration threshold limits.

INTRODUCTION

Catalytic and solid state properties of MoO_3–Al_2O_3 systems have been the subject of numerous investigations in the past, thus making it difficult to give a comprehensive review of this broad field. Moreover, there are only few cases (*1–3*) among the variety of reactions studied wherein significant relationships between solid state properties and catalytic activity have been outlined. To contribute to the question and to clear up some aspects concerning the nature of active sites in relation to the catalytic activity we have investigated a series of supported as well as coprecipitated MoO_3·Al_2O_3 catalysts; proper choice of the support has allowed studies of compositions up to 30 wt% MoO_3, exceeding the limits (15–20% at most) found in previous work (*2, 4–8*). In this paper we limit ourselves to present results on fresh catalysts, i.e., on the oxidized state; properties of MoO_3·Al_2O_3 following reduction or outgassing are discussed in a second paper (*9*). Search of suitable model reactions has indicated a variety of interesting cases which will constitute the basis of future papers: among them we have chosen the reactions of propylene as this enables us to differentiate sites active in the disproportionation reaction and formation of acetone (*10, 11*).

EXPERIMENTAL METHODS

Preparation of Samples

Alumina-supported catalysts containing 2 to 30 wt% MoO_3 were prepared by the impregnation technique. Calculated amounts of $(NH_4)_6Mo_7O_{24}$·$4H_2O$ (Kuhl-

* Present address: Montedison Research Laboratories, Priolo (Sicily).

mann) were dissolved in a volume of H_2O and H_2O_2 (pH 3.9–4.9 for 2–30 wt% MoO_3) corresponding to the total pore volume of the BASF γ-Al_2O_3 (A.P.S. = 70 μm, boehmite structure) to be impregnated. After 2 hr of standing, the impregnate was air-dried for 14 hr at 110°C, and finally calcined at 500°C for 8 hr in air, or otherwise under conditions explicitly stated. The final Mo content of the samples was verified by atomic absorption techniques.

Samples of coprecipitated catalysts were prepared by bringing to dryness aqueous solutions of $Al(NO_3)_3 \cdot 9H_2O$ and $(NH_4)_6Mo_7O_{24} \cdot 4H_2O$ in calculated amounts followed by calcination in air to constant weight (8 hr) at 500, 700 or 900°C.

Reference to the various samples will be made by giving their composition as wt% MoO_3 followed by the temperature of pretreatment: hence MoO_3-4-500 means a sample of MoO_3 supported on Al_2O_3, having 4% of the active element as MoO_3, heat-treated at 500°C. Samples of $Al_2(MoO_4)_3$ are simply indicated by the symbol AlMo and the temperature of final treatment.

Physicochemical Characterization

1. X-Ray Powder Analysis

A standard Philips X-ray diffractometer PW 1050/1051/4082 was used with Cu $K\alpha$ radiation, $\lambda = 1.5418$ Å. The diffraction angle indicator of the goniometer (2θ) was calibrated by the (111), (311) and (620) reflections of a silicon standard. Spectra of finely ground samples were run in the 2θ range 5–80°.

2. DTA and TG Analysis

DTA measurements were carried out on a Du Pont 950 apparatus equipped with high and medium T cells, using calibrated Pt–10% Rh and Cr–Al thermocouples. As reference sample, Al_2O_3 calcined at 1000°C was used. All experiments were run in air, at atmospheric pressure at a heating velocity of 15°C min^{-1}. In the TG experiments ca. 120 mg of the sample were heated in a dry air flux (60 cm^3 min^{-1}) at the same heating velocity as above, until constant weight was attained.

3. Optical Microscopy

Measurements were carried out with a polarizing Ortholux Leitz microscope, with up to $10^3\times$ magnification.

4. Infrared Spectroscopy

Transmittance spectra for powdered samples (<100 mesh) were recorded in the range 1000–400 cm^{-1} on a Perkin-Elmer 225 spectrophotometer using Nujol mulls. Reflection spectra were recorded in the same range by the multireflection a.t.r. technique (attenuated total reflectance) for catalyst specimens with the original particle size distribution.

5. Diffuse Reflectance Spectroscopy

Diffuse reflectance spectra of the original and finely ground catalyst samples were recorded in the range 210–700 nm by use of a Perkin-Elmer Hitachi-EPS 3T spectrophotometer attachment against standards of Al_2O_3.

6. Surface Area, Pore Volume, Pore Size Distribution and Chemical Density

Surface areas were calculated from N_2 adsorption isotherms at 77°K (standard value 16.2 $Å^2$ for the N_2 molecule) using a flow apparatus. Pore volumes and pore size distribution were determined by means of a mercury porosimeter Carlo Erba Model AG 60 and 70H for the 1000 and 2000 atm range, respectively. Chemical densities were measured by a Beckmann pycnometer Model 900 using a He stream.

7. Solubility

The amounts of free and chemically combined MoO_3 were obtained by treating a known quantity of the catalysts with diluted ammonia (3 wt%) in which MoO_3 dissolves, due to its acid character, while molybdates and other solid–solid interaction products are insoluble. The Mo content of the filtrate was determined by atomic absorption spectrophotometry (Perkin-Elmer Model 303). Variation of the ammonia concentration was found not to influence the results.

RESULTS

1. X-Ray Powder Spectra

a. Mechanical Mixtures of MoO_3 and γ-Al_2O_3

X-Ray powder spectra reveal the presence of both components in all samples examined, from 2 to 30 wt% MoO_3.

b. Supported Catalysts

Powder spectra of all catalyst samples dried at 110°C show the presence of microcrystalline γ-Al_2O_3 (ASTM 10-425) and absence of the characteristic diffraction bands of MoO_3; in the 20–30 wt% samples weak diffraction bands were found which were attributed to salt deposition.

After additional calcination, evidence for the presence of crystalline MoO_3 was found in the MoO_3-30-350, MoO_3-25-450 and MoO_3-30-450 samples, together with a microcrystalline phase, probably $Al_2(MoO_4)_3$, in the latter two samples. Catalysts of the 500°C series have similar spectra, the main difference being net evidence for Bragg reflections of $Al_2(MoO_4)_3$ in MoO_3-30-500. In the 700°C series MoO_3 is absent; $Al_2(MoO_3)_4$ is observed at a lower MoO_3 limit (MoO_3-15); its intensity was maximum at MoO_3-30-700.

c. Calcined Aluminum Molybdate

The X-ray powder spectrum of the AlMo-500 series indicates the presence of unreacted MoO_3 together with the reaction product $Al_2(MoO_4)_3$. After additional calcination at 700 and 900°C the diffraction bands of MoO_3 fall below the detection level while the $Al_2(MoO_4)_3$ reflections increase in intensity. The spectrum is interpretable on the basis of an orthorhombic cell (space group *Pnca*, $a = 9.0$, $b = 12.5$, $c = 9.0$ Å).

d. Activated Alumina Samples

X-ray powder photographs of the calcined alumina samples (500°C) were similar to Stumpf and co-workers' (*12*) γ-alumina.

2. DTA and TG Analysis

DTA of an MoO_3-30-110 sample shows an endothermal transformation at 248°C, followed by an endothermal drift of the base line at about 410°C; no further transformation is observed till 800°C. The results agree with those reported in Ref. (*13*) where a reaction temperature between 300 and 400°C has been indicated, depending upon the composition of the catalysts (endothermic peak close to 400°C for the 30 wt% $MoO_3 \cdot Al_2O_3$ mixture). X-Ray diffraction at room temperature (RT) of the same sample heated up to 470°C shows the absence of diffraction bands of MoO_3 and the onset of $Al_2(MoO_4)_3$ formation.

TG analysis was used to study the degree of hydration of various samples, following conditioning in air, at RT, for long periods of time. Weight losses per unit weight of Al_2O_3, shown in Fig. 1 (heating rate: 15°C/min, in dry air) for the samples calcined at 500°C, indicate higher hydration capacities of MoO_3-containing samples with respect to γ-Al_2O_3; the extent of hydration is roughly proportional to the MoO_3 content and involves 2 moles of H_2O per MoO_3.

3. Optical Microscopy

In accordance with the results of X-ray powder spectra, three distinct phases were

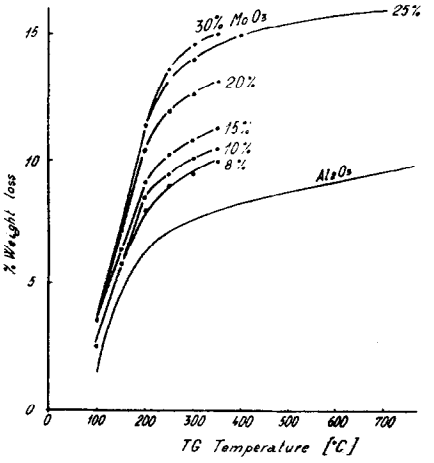

FIG. 1. Variation with temperature of percentage weight loss (as H_2O) referred to unit weight of Al_2O_3, in TG analysis of various MoO_3/Al_2O_3 samples of the 500°C series.

found in the AlMo-500 samples, indicating incomplete reaction; after calcination at 700°C the sample is composed of homogeneous crystalline aggregates with refractive index n in the 1.90–1.99 interval.

Examination of the 500°C supported catalysts showed that the active component is distributed uniformly over the granules with the elemental particle sizes below the resolving power of the microscope (<0.2 μm). The mean refractive index of the granules increases gradually from 1.64 in alumina to 1.66 in MoO_3-rich catalysts. The MoO_3-30-500 sample presents superficial crystallization of MoO_3.

4. Infrared Spectra

Intensities of the various Mo–O frequencies recorded by the a.t.r. and transmittance techniques are given for the MoO_3-500 series (Table 1); slight differences are apparent in case of model compounds, at variance with supported catalysts, which show distinct surface and bulk structures. Starting from transmittance spectra, we notice for supported catalysts up to 20 wt% of MoO_3 the intense absorption of Al_2O_3 (plateau in the 940–520 cm^{-1} region) covering any diagnostic Mo–O frequency of the bulk. In the same region a.t.r. spectra reveal, on the contrary, the existence of molybdenum species at the surface of the catalysts already at the lowest MoO_3 content, as indicated by the absorption band near 800 cm^{-1} which displays maximum intensity near the MoO_3-10 content. Further increase of MoO_3 leads to other absorptions which concentrate in a broad band in the 900 cm^{-1} region; simultaneously the 800 cm^{-1} band becomes relatively less important.

In the highest MoO_3 region (25–30 wt% MoO_3) the following observations are relevant: (a) The 900 cm^{-1} band resolves into a set of intense components at 800, 830, 880 and 900 cm^{-1}, the most important being the 900 cm^{-1} (a.t.r. spectra). (b) The transmittance spectrum of MoO_3-30-500 is different from the a.t.r., showing absorption above 900 cm^{-1}, which is attributable to free MoO_3 present in the bulk. (c) Both transmittance and a.t.r. spectra of the catalysts show absorption at 630 cm^{-1}, absent in model compounds (Table 1).

Following literature information (*15*) the 800 cm^{-1} absorption is diagnostic of Mo–O_t

TABLE 1

INFRARED FREQUENCIES (cm^{-1}) OF MoO_3/Al_2O_3 CATALYSTS AND SOME MODEL COMPOUNDS[a]

Compound	A.t.r. spectrum	Transmittance spectrum
Model compounds		
$Al_2(MoO_4)_3$ 900°C	935(s), 890(s), 865(vs) 830(s), 815(s)	920(vs), 860(s), 830(s) 815(s), 440(s)
MoO_3	990(s), 855(vs), 815(s)	990(s), 860(vs), 820(m) 540(s)
Al_2O_3	Plateau 940–520 ca. 800(sh)	Plateau 940–520
Catalysts		
MoO_3-4-500	800(s)	Plateau 940–520
MoO_3-8-500	800(s)	Plateau 940–520
MoO_3-10-500	800(s)	Plateau 940–520
MoO_3-15-500	ca. 900(b), 800(s)	Plateau 940–520
MoO_3-20-500	900(s), 885(s), 800(m)	Plateau 940–520
MoO_3-25-500	900(vs), 885(s), 830(s) 800(m), ca. 630(b)	ca. 900(vs,b), 850(m) 630(w)
MoO_3-30-500	900(vs), 880(s), 830(s) 800(w), ca. 630(b)	980(m), 920(sh), 860(s) 570(s)

[a] vs, very strong; s, strong; m, medium; w, weak; sh, shoulder; b, broad.

bonds in a tetrahedral [MoO_4] oxomolybdenum(VI) arrangement, as in $CaMoO_4$, with four terminal oxygens (O_t) at the Mo atom. As to the 900 cm^{-1} region, various interpretations are possible (*15*), as discussed below; altogether the complexity of the spectra in this region suggests less terminal O_t and more bridged O_b bonds, both in tetrahedral and octahedral configurations. Finally, the infrared spectrum of $Al_2(MoO_4)_3$ is rather simple, showing intense absorptions only in the 930–815 cm^{-1} region and at 440 cm^{-1}: on the basis of literature information (*14*, *15*) it is in better agreement with a tetrahedral [MoO_4] arrangement.

5. *Electronic Spectra*

Reflectance spectra recorded in the range 210–360 nm using samples with the original granulometry are shown in Figs. 2–6; no absorption bands were found in the region 360–700 nm. Interpretation of spectra followed diagnostic criteria indicated in the literature (*5*, *16*, *17*) and comparison with spectra of model compounds (Fig. 2). On this basis, absorption in the 260–280 nm region was attributed to tetrahedral Mo(VI) and the 300–320 nm band to octahedral Mo(VI). Comparison with model compounds (see A, B and C in Fig. 2) further suggests that the 225 nm band already claimed as indicative of tetrahedral molyb-

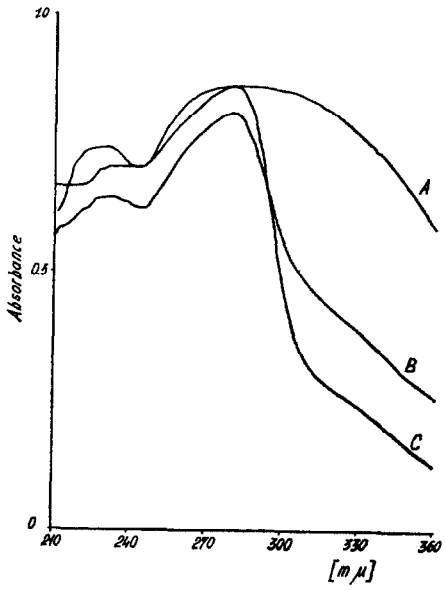

FIG. 3. Ultraviolet reflectance spectra of $Al_2(MoO_4)_3$ samples: (A) AlMo-500, (B) AlMo-700, (C) AlMo-900.

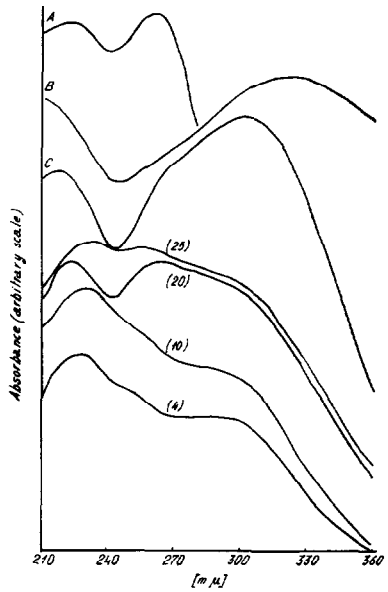

FIG. 2. Ultraviolet reflectance spectra of reference compounds [(A) $Na_2MoO_4 \cdot 2H_2O$, (B) MoO_3, (C) $K_2O \cdot 2MoO_3$ (500°C, 8 hr)] and of MoO_3/Al_2O_3 samples of the 500°C series (8 hr) after leaching with NH_4OH (3%) (in brackets the wt% MoO_3).

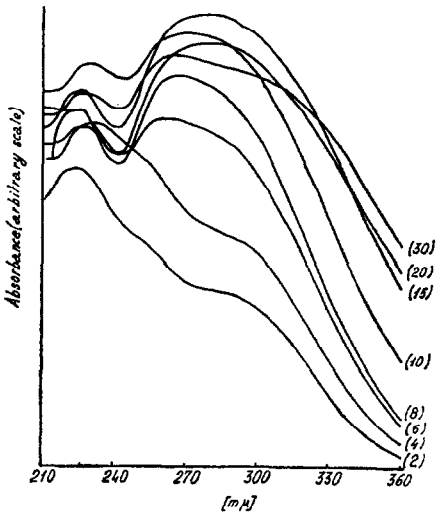

FIG. 4. Ultraviolet reflectance spectra of MoO_3/Al_2O_3 samples of the 500°C series (8 hr) (in brackets the wt% MoO_3).

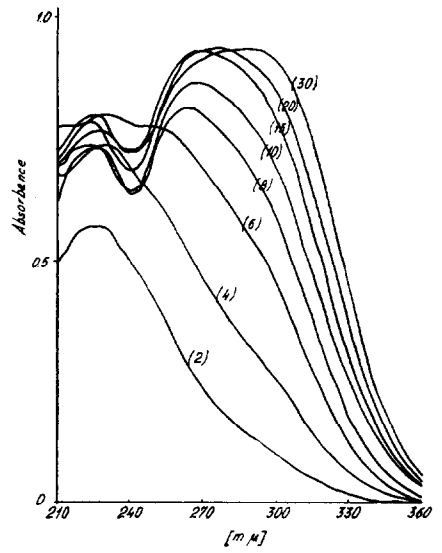

FIG. 5. Ultraviolet reflectance spectra of MoO_3/Al_2O_3 samples of the 110°C series (12 hr) (in brackets the wt% MoO_3).

denum is also in common with octahedral configurations and therefore cannot be used for diagnostic purposes. Adoption of these criteria in the case of $Al_2(MoO_4)_3$ (Fig. 3) confirmed, at least for the samples calcined at 700 and 900°C, the tetrahedral coordination already indicated by infrared; the

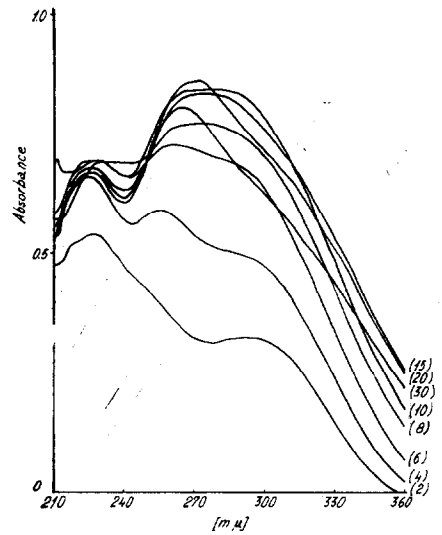

FIG. 6. Ultraviolet reflectance spectra of MoO_3/Al_2O_3 samples of the 700°C series (8 hr at 500°C and 4 hr at 700°C) (in brackets the wt% MoO_3).

extra absorption component at about 300 nm in the spectrum of the AlMo-500 sample reveals also some octahedral molybdenum in accordance with the incompleteness of the solid–solid interaction already evidenced by X-ray analysis.

With regard to the supported catalysts, the effect of composition is better illustrated with reference to the MoO_3-500 supported series (Fig. 4); thus while the spectra of MoO_3-2-500 and MoO_3-4-500 samples clearly delineate the contribution of three components at 225, 255 and 300 nm, in MoO_3-richer samples the shoulder at 255 nm develops in intensity with respect to the 225 nm band and leads to a well-defined peak at 265 nm. At even higher MoO_3 contents a second shoulder at 300 nm develops, causing the 265 nm peak to broaden to give a composite band in the 265–300 nm interval, until in MoO_3-30-500 the 265 and 310 nm components are again resolved. Although no quantitative assignment can be based on the relative peak intensities it is suggested that molybdenum(VI) on the surface of the catalysts calcined at 500°C is initially tetrahedrally coordinated, evolving towards a higher octahedral/tetrahedral ratio at increasing Mo-contents in the system.

A comparison of the reflectance spectra in terms of the temperature of activation (Figs. 4–6) using the MoO_3-500 series as reference shows the minor presence of the octahedral Mo(VI) species in all catalysts calcined at lower temperatures (MoO_3-110), as the 300 nm component is quite low (Fig. 5). On the contrary, at higher temperatures (MoO_3-700) the octahedral component is pronounced already in the low MoO_3 region (up to about 8 wt%), diminishing at compositions exceeding MoO_3-15-700 (Fig. 6) at the expense of a strong increase of tetrahedral Mo(VI) as in $Al_2(MoO_4)_3$, characterized by the 265 nm band.

Variations produced upon treatment with diluted ammonia are shown in Fig. 2; comparison with untreated samples (Fig. 4) shows a decrease of the 300 nm component in the 10–30 wt% range indicating preferential removal of octahedral species.

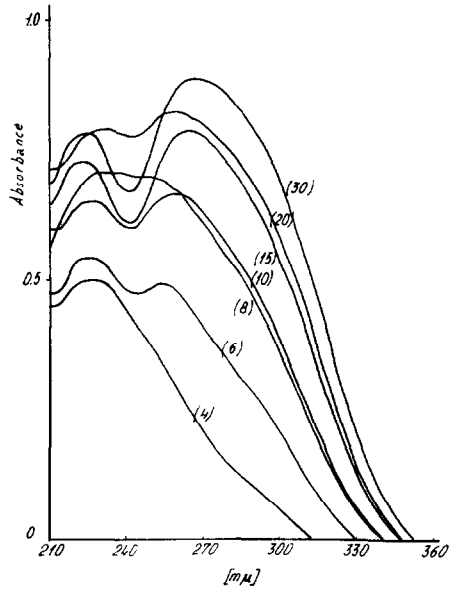

FIG. 7. Ultraviolet reflectance spectra of MoO_3/Al_2O_3 samples of the 110°C series, after grinding (in brackets the wt% MoO_3).

Differences between bulk and surface properties were demonstrated by a series of reflectance spectra using finely powdered samples: spectra of catalysts dried at 110°C show a higher contribution of octahedral species at the surface than in the bulk (Figs. 5, 7), while no appreciable difference was noticed in the 500 and 700°C series.

6. *Surface Areas, Pore Volumes, Mean Pore Radii and Chemical Densities*

Surface areas (SA), pore volumes (V_p) and chemical densities (ρ_t) for samples of the MoO_3-500 series are given in Table 2 together with the calculated values of the mean pore radii ($r = 2\ V_p/SA$). Values of SA for the 500 and 700°C samples are plotted in Fig. 8 against values calculated on the basis of the contribution of γ-Al_2O_3 only: comparison shows little variations for the MoO_3-500 series with a reproducible discontinuity at 8 wt% and an almost linear decrease in the range 10–30 wt% MoO_3. For samples of the MoO_3-700 series deviations from linearity are much larger and are accompanied by two characteristic points of discontinuity, at MoO_3-2 and MoO_3-15, respectively.

As for AlMo samples, they are characterized by a lower pore volume and very low surface area, which result in a much higher value of the mean pore radius.

TABLE 2
CHEMICAL–PHYSICAL CHARACTERISTICS OF MoO_3/Al_2O_3 CATALYSTS ACTIVATED AT 500°C FOR 8 HR IN AIR

Catalyst	Surface area (m^2/g)	Pore vol[a] (cm^3/g)	Mean pore radius[a] (Å)	Pore vol[b] (cm^3/g)	Mean pore radius[b] (Å)	Chemical density (g/cm^3)
Al_2O_3-500	216	0.94	87	1.24	115	3.08
MoO_3-2-500	202	0.92	91	1.20	118	3.03
MoO_3-4-500	205	0.96	94		(115)[c]	
MoO_3-6-500	211	0.93	88		(111)	3.22
MoO_3-8-500	185	0.87	94		(123)	
MoO_3-10-500	196	0.91	93		(114)	3.33
MoO_3-15-500	183	0.82	89	1.03	113	3.44
MoO_3-20-500	169	0.85	101		(116)	3.52
MoO_3-25-500	156	0.71	90		(119)	
MoO_3-30-500	129	0.76	117	0.87	135	3.43
AlMo-500	12.0	0.50	835			3.70
AlMo-700	1.3	0.44	6750			

[a] Referred to 1000 atm.

[b] Referred to 2000 atm.

[c] The values in parentheses were calculated from the experimentally determined surface areas (column 1) and from extrapolated values of the pore volumes (column 4).

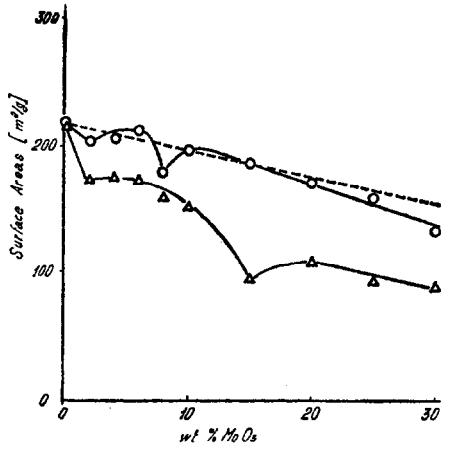

FIG. 8. Surface areas as a function of the composition: (○) MoO_3-500, (△) MoO_3-700.

7. *Solubility*

Results of analyses of the solubility in ammonia are reported in Table 3 together with those of Ishii and Matsuura (*18*) for coprecipitated catalysts: in both cases the catalysts appear to contain very considerable amounts of extractable MoO_3 and relatively small amounts of MoO_3 combined to the carrier. Table 3 suggests also that for any specific composition up to MoO_3-30 more MoO_3 is combined by impregnation than by coprecipitation; moreover, variations of the mole fraction of combined MoO_3 with the composition indicate also that in case of coprecipitated systems the combined MoO_3 increases more than linearly with the MoO_3 content.

DISCUSSION

An important point of discussion is whether MoO_3 is present on the surface of the support as a monolayer, as a distinct phase in the form of clusters, or as interaction products with the carrier. Surface areas and pore volumes of MoO_3-500 samples up to 15–20 wt% MoO_3 favor undoubtedly the monolayer deposition as they fit closely values calculated on the basis of the contribution of the support only (Fig. 8). In catalysts with more than 20 wt% MoO_3 and on all samples of the MoO_3-700 series the increase of the mean pore radius and surface area below calculated values for the monolayer suggests other processes which X-ray diffraction helps to identify as formation of a well-defined compound, $Al_2(MoO_4)_3$. Clustering as free MoO_3 is excluded, except for the MoO_3-30-500 sample, by X-ray diffraction and ir reflectance and transmittance spectra.

TABLE 3
RESULTS OF SOLUBILITY EXPERIMENTS IN 3 wt% AMMONIA

Catalyst	Impregnation[a] % MoO_3 Extracted	Impregnation[a] % MoO_3 Combined	Impregnation[a] Moles MoO_3 combined/mole Al_2O_3	Coprecipitation[b] (moles MoO_3 combined/mole Al_2O_3)
MoO_3-4-500	67	33	0.010	—
MoO_3-8-500	74	26	0.016	—
MoO_3-10-500	73	27	0.021	—
MoO_3-13.6-500	—	—	—	0.017
MoO_3-15-500	74	26	0.032	—
MoO_3-20-500	75	25	0.044	—
MoO_3-25-500	79	21	0.049	0.036
MoO_3-30-500	87	13	0.040	—
MoO_3-59-500	—	—	—	0.066
MoO_3-76-500	—	—	—	0.142
MoO_3-81-500	95	5	0.170	—
MoO_3-85-500	—	—	—	0.232

[a] Samples activated 8 hr in air at 500°C (present work).
[b] Samples activated 24 hr in air at 500°C [Ref. (*18*)].

Thus, depending upon the composition, the system appears to obey closely the monophase model as in the cases discussed by Lipsch (*7*) and Kabe *et al.* (*19*), or it is characterized by the occurrence of chemical interaction leading to $Al_2(MoO_4)_3$ as observed by Asmolov and Krylov (*5*).

With regard to the nature and the extent of the processes underlying the formation of a monolayer, consider the heptamolybdate ion, $[Mo_7O_{24}]^{6-}$, in ammonium paramolybdate solutions, under the preparative conditions of pH (3.9–5.0) and concentration (2×10^{-2}–4×10^{-1} *M*). During the process of impregnation this ion is subject to the following equilibrium

$$Mo_7O_{24}^{6-} + 4\ H_2O \rightleftharpoons 7\ MoO_4^{2-} + 8\ H^+,$$

so already in this stage one can expect various degrees of (dis)aggregation of the ions adsorbed on the surface, depending upon starting concentration and pH of the solution. The effect is evident on samples activated at 110°C (Fig. 5) which show tetrahedral monomeric $[MoO_4]^{2-}$ groups within a wide range of ammonium paramolybdate concentrations largely exceeding polyanionic species with complex groupings of $[MoO_6]$-octahedra. Interaction with the support undoubtedly involves surface OH groups which are generally accepted as the reactive sites (*20*), also in agreement with recent results of Dufaux, Che and Naccache (*21*) based on the reaction of TCNE with $MoO_3 \cdot Al_2O_3$ samples. Thus the first step in the sequence should be the creation of structures before calcination such as:

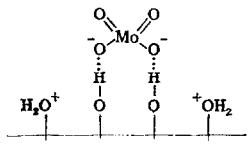

The existence of these and other similar intermediate complexes exhibiting weak bonding only, is supported experimentally by TG data which indicate that the rehydration capacities and dehydration rates of the catalysts are higher than those of Al_2O_3 (Fig. 1). Subsequent activation is expected to lead, via condensation reactions of molybdate ions with surface OH groups of the support, to the formation of stable alumina–molybdic acid complexes, such as:

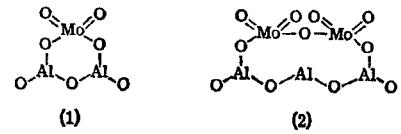

(1) (2)

where (**1**) and (**2**) are monomeric and dimeric surface structures, respectively. Possible variants arising from: (a) different degrees of hydration of the support and dispersed molybdic anhydride crystallites (e.g., in MoO_3-rich catalysts); (b) fully dehydrated molybdenum trioxide (at temperatures over about 500°C) reacting with randomly distributed surface hydroxyl groups, might lead to polymeric structures such as (**3**) and (**4**), respectively:

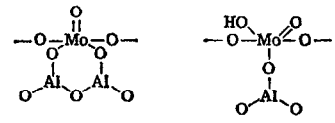

(3) (4)

Interaction processes as indicated above can be rationalized in terms of two main factors: surface coverage by OH groups (θ_{OH}) and ratio $[MoO_3]$/[surface OH groups]. With respect to the former, the influence of the temperature of activation seems obvious: simple calculations based on TG data show θ_{OH} of the order of 37% of a monolayer for the 500°C samples and 14% for the 700°C samples, in good agreement with estimates for similar γ-Al_2O_3 structures (*22*). While these figures fix only the maximum allowable degree of occupation of the surface, the configuration of Mo–oxo species must be dictated by the availability of OH groups with respect to MoO_3. This aspect is illustrated by considering complete coverage of all accessible OH groups: for samples calcined at 500°C it would involve an estimated 11.4 wt% MoO_3 (per 100 g of total catalyst) in case of Mo bonded to the surface as in (**1**) and (**3**) (OH/Mo = 2), or about 20.4% for (**2**) and (**4**) (OH/Mo = 1). For MoO_3-

700, these values become 4.6 and 8.8%, respectively. The formation of dimeric and polymeric surface structures (**2**) and (**4**) is then favored at more dehydrated alumina samples, thus at higher temperature as well as at higher MoO_3 contents.

X-Ray and spectral evidence agrees with expectations, indicating progressive changes in the structure of the surface species with temperature and MoO_3 content.

As to the influence of temperature, compositions in the range up to 8–10 wt% MoO_3 are characterized by progressive condensation of tetrahedral $[MoO_4]^{2-}$ groupings as temperature is increased, leading to lower threshold limits of octahedral polymeric forms (Figs. 4–6). At higher MoO_3 contents octahedrally coordinated oxomolybdenum species, still present at low temperature (110°C), further increase up to 500°C; a sharp reversal of the tendency sets in at 700°C, when bulk $Al_2(MoO_4)_3$ is formed with tetrahedral Mo(VI).

With regard to the influence of MoO_3 concentration, at otherwise identical conditions of preparation and activation, mainly tetrahedral Mo(VI) species are found at the lower contents and octahedral Mo(VI) species at higher MoO_3 contents; at the highest MoO_3 concentrations, tetrahedral Mo(VI) due to $Al_2(MoO_4)_3$ is present. Taking the MoO_3–500 series as reference, we notice at the lowest compositions (up to 4 wt%) the strong 800 cm^{-1} a.t.r band and 265 nm reflectance band characteristic of tetrahedral Mo(VI) with 4 Mo–O_t bonds (*15*), thus suggesting a highly dispersed state of Mo in the form of $[MoO_4]^{2-}$ species. At increasing molybdenum contents (up to 10–15 wt%) the development of the 800 cm^{-1} (a.t.r.) band and the onset of the 900 cm^{-1} band (Table 1) and of the 265–300 nm reflectance band (Fig. 4) suggest progressive increase of structures with bridged oxygens in mixed tetra- and octahedral Mo(VI) geometries, such as 1 Mo–O_b and 3 Mo–O_t bonds in tetrahedra or fewer Mo–O_t and more Mo–O_b in octahedra. In the MoO_3-rich region (>15% MoO_3) the prevailing octahedral configuration cannot simply be attributed to free MoO_3 because of the absence of the strong 990 cm^{-1} Mo–O_t stretching vibration in the a.t.r. spectra and of the diffraction bands of MoO_3 in the X-ray powder spectra. Other possibilities for octahedral Mo(VI) readily suggest themselves. One is polymeric structures such as (**3**) and (**4**), resulting from the interaction of molybdenum trioxide with fewer surface OH groups or from progressive condensation of tetrahedral groupings. A second possibility is that Mo(VI) occupies octahedral cation sites in the defect spinel lattice of γ-Al_2O_3 (*23*). The basic mechanism of incorporation of Mo ions might be similar to that first discussed by Kordes (*24*) for γ-Al_2O_3 containing small amounts of lithium and by Tomlinson *et al.* (*25*) for cobaltous ions impregnated on Al_2O_3: the process, which involves primarily the bulk, is expected to occur once the residual surface OH groups are exhausted (*21*) and lead to a modification of the unit-cell size and surface areas as discussed by Levy (*26*) and Levy and Bauer (*27*).

On the basis of the results discussed above, both possibilities appear acceptable in our $MoO_3 \cdot Al_2O_3$ system. In the case of polymeric forms such as (**3**) and (**4**), distinguishing characteristics in the infrared spectra are the increased absorptions at 885 and 830 cm^{-1} known to be due to continuous Mo–O–Mo bonds (*15*, *28*, *29*). As to the 900 cm^{-1} band, it can be ascribed either to the ν_1 frequency of tetrahedra or to dioxomolybdenum species containing *cis*-MoO_2 groups as in $MoO_2(OH)_2$ (*30*, *31*). The latter assignment will be discussed further in connection with results on reduced samples (*9*).

With regard to molybdenum incorporated in alumina vacancies, the 630 cm^{-1} band, which is not attributable to $Al_2(MoO_4)_3$, appears to be diagnostic, as recent literature (*28*) ascribes it to vibrations in an octahedral Mo(VI) oxygen structure like $CoMoO_4$. Proof in favor of incorporation of molybdenum into the AlO_6 vacancies can be inferred also from trends in surface areas (Fig. 8).

The two alternatives, polymeric $[MoO_6]$ on the surface and $[MoO_6]$ incorporated in the lattice, should be considered as dif-

fering only in topochemical respects, as they represent different locations, namely at or under the outermost layers of the catalyst. It is possible that they act, by ion diffusion processes, as precursors of the thermo-dynamically most stable phase in the system, $Al_2(MoO_4)_3$. This assumption is supported by the observation that the threshold of octahedral species always occurs at lower composition levels than $Al_2(MoO_4)_3$, as indicated by X-ray diffraction, uv and ir spectra. Furthermore, formation of $Al_2(MoO_4)_3$ is favored by increasing temperature as it is detected at MoO_3-15-700 as against MoO_3-30-500; similar considerations apply to $[MoO_6]$ in the octahedral vacancies as diagnosed from the detection limits of the 630 cm^{-1} a.t.r. band for the 700 and 500°C series, respectively.

With regard to the fraction of MoO_3 going to $Al_2(MoO_4)_3$, solubility data (Table 3) prove undoubtedly that formation of $Al_2(MoO_4)_3$ is slow: these results agree with the absence of well-defined peaks in the DTA analysis, indicating that the interaction MoO_3/Al_2O_3 leading to $Al_2(MoO_4)_3$ requires a large temperature interval in order to go to completion.

Conclusions

This study has provided a comprehensive picture of the generation of molybdenum species on impregnated γ-Al_2O_3 samples both on the surface and in the bulk, as a function of the MoO_3 concentration and calcination temperature. The main feature of uncalcined catalyst samples are chemisorbed molybdenum species at the surface. Evidence has been presented for the existence, in calcined samples, of monomers (tetrahedra) on catalyst surfaces exhibiting a high percentage of OH groups; on partially depleted samples dimeric and polyanionic oxomolybdenum(VI) species are present either as $[MoO_6]$ on the surface or incorporated in octahedral interstices of γ-Al_2O_3 when surface OH groups are no longer available. The octahedral species and the chemically well-defined phase, $Al_2(MoO_4)_3$, increase with higher molybdenum concentration and calcination temperature.

Acknowledgment

Thanks are due to Professor R. Ugo for helpful discussions.

References

1. John, G. S., Den Herder, M. J., Mikovsky, R. J., and Waters, R. F., *in* "Advances in Catalysis" (D. D. Eley, W. G. Frankenburg, V. I. Komarewsky and P. B. Weisz, Eds.), Vol. 9, p. 252. Academic Press, New York, 1957.
2. Seshadri, K. S., and Petrakis, L., *J. Phys. Chem.* **74**, 4102 (1970).
3. Boreskov, G. K., Dzis'ko, V. A., Emel'yanova, V. M., Pecherskaya, Y. I., and Kazanskii, V. B., *Dokl. Akad. Nauk SSSR* **150**, 829 (1963).
4. Naccache, C., Bandiera, J., and Dufaux, M., *J. Catal.* **25**, 334 (1972).
5. Asmolov, G. N., and Krylov, O. V., *Kinet. Katal. (USSR)* **11**, 1028 (1970).
6. Masson, J., and Nechtschein, J., *Bull. Soc. Chim. Fr.* 3933 (1968).
7. Lipsch, J. M. J. G., PhD thesis, Technische Hogeschool Eindhoven, 1968: reprinted by Climax Molybdenum Co.
8. Krylov, O. V., and Margolis, L. Y., *Kinet. Katal.* **11**, 432 (1970).
9. Giordano, N., Castellan, A., Bart, J. C. J., Vaghi, A., and Campadelli, F., unpublished data.
10. Giordano, N., Padovan, M., Vaghi, A., Bart, J. C. J., and Castellan, A., unpublished data.
11. Giordano, N., Vaghi, A., Bart, J. C. J., and Castellan, A., unpublished data.
12. Stumpf, A., Russell, A. S., Newsome, J. W., Tucker, C. M., *Ind. Eng. Chem.* **42**, 1398 (1950).
13. Ogasawara, S., Nakada, Y., Iwata, Y., and Sato, H., *Kogyo Kagaku Zasshi* **73**, 509 (1970).
14. Caillet, P., and Saumagne, P., *J. Mol. Struct.* **4**, 351 (1969).
15. Mitchell, P. C. H., and Trifiró, F., *J. Chem. Soc., Ser. A* 3183 (1970).
16. Ashley, J. H., and Mitchell, P. C. H., *J. Chem. Soc., Ser. A* 2821 (1968).
17. Ashley, J. H., and Mitchell, P. C. H., *J. Chem. Soc., Ser. A* 2730 (1969).
18. Ishii, Y., and Matsuura, I., *Technol. Rep. Kansai Univ.* **10**, 47 (1969).
19. Kabe, T., Yamadaya, S., Oba, M., and Miki, Y., *Int. Chem. Eng.* **12**, 366 (1972).
20. Peri, J. B., *J. Phys. Chem.* **69**, 220 (1965).

21. DUFAUX, M., CHE, M., AND NACCACHE, C., *J. Chim. Phys. Physicochim. Biol.* **67,** 527 (1970).
22. HENDRIKSEN, B. A., PEARCE, D. R., AND RUDHAM, R., *J. Catal.* **24,** 82 (1972).
23. SINHA, K. P., AND SINHA, A. P. B., *J. Phys. Chem.* **61,** 758 (1957).
24. KORDES, E., *Z. Kristallogr.* **91,** 193 (1935).
25. TOMLINSON, J. R., KEELING, R. O., RYMER, G. T., AND BRIDGES, J. M., *Actes Congr. Int. Catal., 2nd,* 1960 p. 1831 (1961).
26. LEVY, R. M., *J. Catal.* **8,** 87 (1967).
27. LEVY, R. M., AND BAUER, D. J., *J. Catal.* **9,** 76 (1967).
28. CLARK, G. M., AND DOYLE, W. P., *Spectrochim. Acta* **22,** 1441 (1966).
29. MATTES, R., AND SCHRODER, F., *Z. Naturforsch. B* **24,** 1095 (1969).
30. MOORE, F. W., AND RICE, R. E., *Inorg. Chem.* **7,** 2510 (1968).
31. MITCHELL, P. C. H., *Quart. Rev.* **20,** 103 (1966).